UNIVERSIDADE ESTADUAL DE CAMPINAS
SISTEMA DE BIBLIOTECAS DA UNICAMP
REPOSITÓRIO DA PRODUÇÃO CIENTIFICA E INTELECTUAL DA UNICAMP

Versão do arquivo anexado / Version of attached file:

Versão do Editor / Published Version

Mais informações no site da editora / Further information on publisher's website:
https://academic.oup.com/treephys/article/43/1/88/6682843

DOI: https://doi.org/10.1093/treephys/tpac105

Direitos autorais / Publisher's copyright statement:
©2022 by Oxford University Press. All rights reserved.

DIRETORIA DE TRATAMENTO DA INFORMAÇÃO

Cidade Universitária Zeferino Vaz Barão Geraldo
CEP 13083-970 – Campinas SP
Fone: (19) 3521-6493
http://www.repositorio.unicamp.br

Tree Physiology 43, 88–101
https://doi.org/10.1093/treephys/tpac105

Research paper

A unit pipe pneumatic model to simulate gas kinetics during measurements of embolism in excised angiosperm xylem

Dongmei Yang[1], Luciano Pereira[2,3], Guoquan Peng[1,4], Rafael V. Ribeiro[2], Lucian Kaack[3], Steven Jansen[3] and Melvin T. Tyree[1,4]

[1]College of Chemistry and Life Sciences, Zhejiang Normal University, Jinhua 321004, China; [2]Laboratory of Crop Physiology, Department of Plant Biology, Institute of Biology, P.O. Box 6109, University of Campinas (UNICAMP), Campinas 13083–970, Brazil; [3]Institute of Systematic Botany and Ecology, Ulm University, Albert-Einstein-Allee 11 Ulm D-89081, Germany; [4]Corresponding authors: G.Peng (penggq@zjnu.cn); M.T.Tyree (mel.tyree@cantab.net)

Received May 24, 2022; accepted August 30, 2022; handling Editor Teemu Holtta

The pneumatic method has been introduced to quantify embolism resistance in plant xylem of various organs by applying a partial vacuum to cut-open xylem. Despite the similarity in vulnerability curves between the pneumatic and other methods, a modeling approach is needed to investigate if changes in xylem embolism during dehydration can be accurately quantified based on gas diffusion kinetics. Therefore, a unit pipe pneumatic (UPPn) model was developed to estimate gas extraction from intact conduits, which were axially interconnected by inter-conduit pit membranes to cut-open conduits. The physical laws used included Fick's law for diffusion, Henry's law for gas concentration partitioning between liquid and gas phases at equilibrium and the ideal gas law. The UPPn model showed that 91% of the extracted gas came from the first five series of embolized, intact conduits and only 9% from the aqueous phase after 15 s of simulation. Considering alternative gas sources, embolism resistance measured with a pneumatron device was systematically overestimated by 2–17%, which corresponded to a typical measuring error of 0.11 MPa for P_{50} (the water potential equivalent to 50% of the maximum amount of gas extracted). It is concluded that pneumatic vulnerability curves directly measure embolism of intact conduits due to the fast movement of gas across interconduit pit membranes, while gas extraction from sap and diffusion across hydrated cell walls is about 100 times slower. We expect that the UPPn model will also contribute to the understanding of embolism propagation based on temporal gas dynamics.

Keywords: angiosperms, embolism, gas diffusion, pneumatic model, pneumatron, unit pipe, vulnerability curves, xylem conduits.

Introduction

According to the cohesion tension theory (CTT), water is transported in land plants under tensile conditions. The CTT has withstood challenges over time (e.g., Benkert et al. 1995) through rebuttals based on reviews of past literature (Tyree 1997), cell pressure probe experiments (Wei et al. 1999) and centrifuge experiments (Cochard et al. 2005). Tensile properties arise in water when confined to xylem conduits, which have pore sizes in pit membranes between 5 and 50 nm, and pore sizes below 2 nm in cell walls (Kaack et al. 2019). The transport system from fine roots to the evaporative surface of leaves is composed of many intact pipes interconnected via pit membranes.

Even though CTT has withstood the test of time, the transport of water under negative pressure is prone to failure (Cochard et al. 2013). Immediately after embolism formation, the conduit fills with a low-pressure void that consists primarily of water vapor. These voids eventually fill up with gas at atmospheric pressure following Henry's law, which describes the nature of the equilibrium between atmospheric gases and gases dissolved in water. One version of Henry's Law can be written as:

$$\frac{[x]_w}{[x]_a} = H^{cc} \quad (1)$$

where $[x]$ represents the mean concentration (mol l^{-1}) of gas x in water, w, or air, a, depending on the subscript. H^{cc} is a constant

© The Author(s) 2022. Published by Oxford University Press. All rights reserved. For permissions, please e-mail: journals.permissions@oup.com

Downloaded from https://academic.oup.com/treephys/article/43/1/88/6682843 by BIBLIOTECA CENTRAL UNIV ESTADUAL CAMPINAS user on 06 February 2025

and approximately 10^{-2} for N_2, O_2 and Ar. The concentration of gas in the air phase comes from the ideal gas law:

$$[x]_a = \frac{n_x}{V} = \frac{P_x}{RT} \quad (2)$$

where n_x is the number of moles of gas x in volume V, P_x is the partial pressure of gas x and RT is the universal gas constant multiplied by temperature in Kelvin.

In xylem conduits of plants, gases can appear after embolism formation events if water remains in the tensile state and disappear if water returns to a non-tensile state slightly below atmospheric pressure. Modeling and experiments have determined the kinetics of bubble disappearance in conduits when the fluid pressure is near or above atmospheric pressure (Tyree and Yang 1992, Yang and Tyree 1992). Recent work has also focused on how long it takes a newly embolized conduit to be fully gas filled, that is, when Ar, O_2 and N_2 reach partial pressures in the conduit equal to those in ambient air. Answers have come from theoretical models and experiments in which the focus has been on the speed of radial gas diffusion between conduits inside stems to the outside surface of the bark (Wang et al. 2015). This radial movement of gas between embolized conduits and the ambient atmosphere is basically controlled by Fick's law of diffusion, which is very slow for the diffusion of gases in water. Hence, even for stems of 10 mm in diameter, the time for equilibrium can be hours to days depending on the diameter and the diffusion coefficient of gases in wet woody stems. In the three studies cited above, axial diffusion was not included in the modeling, and experimental designs for model verification inhibited most of the axial diffusion.

While these former models are useful and interesting, they do not apply to the experimental situation inherent in the pneumatic method (Pereira et al. 2016, Zhang et al. 2018, Jansen et al. 2020, Pereira et al. 2020, Trabi et al. 2021). An automated pneumatron device consists of a gas pressure sensor connected by tubing to the cut end of a shoot with leaves, and it is used to measure the kinetics of gas diffusion from newly embolized, intact vessels to the embolized vessels at the cut surface of a terminal branch. This process involves axial diffusion of gases via hydrated pit membranes (Li et al. 2016, Kaack et al. 2019). Diffusion can be quite quick over the thickness of pit membranes (0.2–1.2 μm). In axial transport, the median time, t_m, for gas to diffuse across a distance s is given by:

$$s^2 = 2D_g t_m \quad (3)$$

where D_g is the coefficient of diffusion of the gas species g (in $m^2\ s^{-1}$), and s is the distance (in m) that half the molecules traverse in time t_m (in s). Gases in water have $D_g = 2 \times 10^{-9}\ m^2\ s^{-1}$, so the time to diffuse through 1 μm of water is approximately 0.25 ms, but the time to diffuse through 0.005 m of water is 6.25×10^3 s ($\cong$1.7 h). Hence, gases spread axially down cut branches more rapidly than radially through stems.

The pneumatic method involves measuring the kinetics of gas movement down the axis of a stem while independently measuring the stem water potential. Since 2016, the pneumatic method has been used to estimate the vulnerability curves (VCs) of woody angiosperms where the interpretation of what is measured is based on qualitative arguments, or by comparing pneumatic VCs to VCs measured by more conventional hydraulic (Pereira et al. 2016, 2020, 2021, Zhang et al. 2018, Chen et al. 2020, Sergent et al. 2020) and non-hydraulic techniques (Chen et al. 2020, Sergent et al. 2020, Guan et al. 2021).

What is clearly lacking in our full understanding of pneumatic measurements is a modeling approach of the gas diffusion kinetics along axial and radial pathways of interconnected conduits, which connects newly embolized, intact conduits with cut-open conduits (Figure 1). Therefore, the purpose of this study is to provide a theoretical background for pneumatic measurements, with the aim of developing a model that quantifies the proportion of embolized conduits, on either a volume basis or hydraulic conductance basis, based on the theoretical kinetics of pressure change via diffusion of gases through intervessel pit membranes. The model presented in this paper complements experimental evidence in recent papers (Pereira et al. 2020, 2021, Sergent et al. 2020, Guan et al. 2021, Paligi et al. 2021). Knowing what is being directly measured in pneumatic experiments on embolism resistance is not only key to incorporate this technique with those from other methods, but will also be essential to understand the gas phase in plants (Gartner et al. 2004, Jansen et al. 2022).

Materials and methods

Model description

Basic concepts of pneumatic measurements The gas pressure in embolized, intact vessels is assumed to be in equilibrium with the ambient air at the beginning of a measuring cycle. In a measuring cycle, a partial vacuum (40 kPa absolute pressure) is drawn in about 1 s at the cut surface of the stem. The stem is connected to a small, known volume of tubing, and this air space is connected to a pressure transducer. Then, the vacuum pump is turned off, and the pressure is monitored every 0.5 s for $<$30 s, during which time the pressure increases by 2–40 kPa to an absolute pressure of 42–80 kPa. This is called the air discharge. At the end of a measuring cycle, the gas pressure is returned to atmospheric pressure for nearly 20 min to ensure that atmospheric pressure has been restored in embolized vessels that are connected to the cut-open vessels. Atmospheric pressure will be achieved quickly in these vessels due to fast axial diffusion through pit membranes in the opposite direction. Intact, isolated embolized vessels that are not in contact with other embolized vessels and cut-open vessels may need hours

Downloaded from https://academic.oup.com/treephys/article/43/1/88/6682843 by BIBLIOTECA CENTRAL UNIV ESTADUAL CAMPINAS user on 06 February 2025

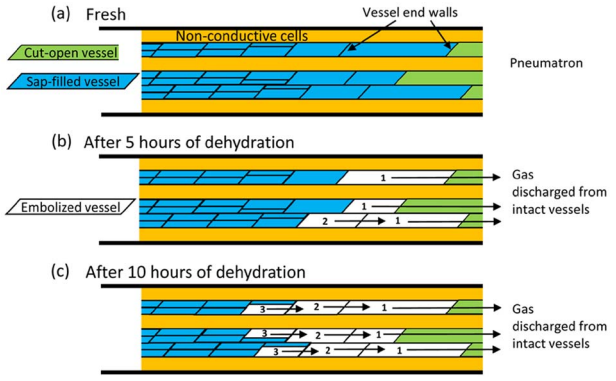

Figure 1. Schematic, two-dimensional representation of the gas pathway during pneumatic experiments in a fresh sample (a) and after 5–10 h of bench dehydration (b and c), with a pneumatron connected on the right, and a terminal, intact branch on the left. Since the cut-open vessels (green color) function as an extension of the discharge reservoir and will very quickly experience the partial vacuum generated by the pneumatron, these vessels do not contribute to estimations of embolism. Gas from intact, embolized vessels (white color), however, is more slowly extracted due to the presence of end walls with intervessel pit membranes. Nevertheless, extraction of gas from intact, embolized vessels is still relatively fast across end walls (black arrows), indicating that the pneumatron is able to directly quantify embolism along a series of few intact vessels. The numbering indicates the consecutive number of a series of embolized, intact vessels.

to reach atmospheric pressure (Wang et al. 2015). Since gas extraction from these isolated vessels would take a very long time, this situation is irrelevant and not included in the unit pipe pneumatic (UPPn) model.

Basic idea of the UPPn model and its assumptions All the theoretical calculations involve Fick's law for the diffusion of gases, Henry's law for gas concentrations at air/water interfaces and the ideal gas law to relate air pressure to gas concentrations. Fick's first law is used in radial or Cartesian coordinates as needed (Crank 1975).

The UPPn model approximates the three-dimensional vessel network in the angiosperm xylem (Zimmermann and Tomlinson 1966). This model may provide a valid approach because the kinetics of axial gas exchange between embolized vessels (pipes) is much faster than that of radial diffusion between any given embolized vessel and the surrounding unembolized, water-saturated, woody tissue. The model simulates the rate of gas extraction axially from embolized vessel lumina to the pressure transducer, and radially from the gas dissolved in the water of the surrounding xylem tissue. Axial transfer of gas occurs between closed (intact) vessels and cut-open vessels via diffusion through water spaces in the cellulose of intervessel pit membranes.

An important assumption in the pneumatic method is that, at the beginning of an experiment, the quantity of gas discharge (measured in pressure change, ΔP) is minimal when there is zero embolism, but rises to a maximum difference when all vessels are embolized. The assumption that there is no or minimal native embolism in plants from the field is reasonable given recent insights into the temporal frequency of embolism (Cochard and Delzon 2013, Dietrich et al. 2019, Guan et al. 2022), and our understanding of hydraulic measuring artifacts (Wheeler et al. 2013, Torres-Ruiz et al. 2017, Lamarque et al. 2018). If the vessel lumina hold only 10% of the water volume of woody stems as based on a 10% vessel lumen fraction (Zanne et al. 2010, Morris et al. 2016), then the embolized vessels will contain approximately 6.0 times more moles of gas than is dissolved in the 5-times-larger water volume surrounding the embolized vessels, based on Henry's constant of air in water, $H^{cc} = 1.85 \times 10^{-2}$. Our model will show that the amount of gas extracted from the water of non-embolized wood is less than 10% of the gas extracted from the embolized vessels during the early part of the 15 s measuring cycle.

We consider in the UPPn model that the primary axial diffusion path follows a single chain of conduits in series, which spans an entire xylem segment. Initially, only the cut-open conduits are embolized, because an air–water meniscus is quickly pulled back into these conduit lumina until it stops at an interconduit pit membrane (Tyree and Zimmermann 2002, Avila et al. 2022). Embolism spreading is then assumed to propagate all the way through a file of conduits in series, resulting in serially arranged ranks of embolized conduits that have axial connectivity with one another via pit membranes. During increased levels of dehydration, more conduits will become embolized, increasing the contiguous pathway for gas movement. This assumption is based on the well-supported evidence that embolism spreads spatially from a previously embolized conduit to an adjacent one, resulting in a non-random pattern, as evidenced by microCT observations of stem xylem (Brodersen et al. 2013, Choat et al. 2016, Wason et al. 2021) and the optical method applied to leaves (Brodribb et al. 2016*a*, 2016*b*, Guan et al. 2021). Although microCT observations have shown embolism formation in isolated conduits not connected to other air-filled conduits (Knipfer et al. 2015, Choat et al. 2016), which could challenge the assumption made here, it is currently unclear how common embolism formation is in isolated vessels of angiosperms due to the small microCT scan volume in relation to vessel length.

Transport and equilibrium coefficients used in the UPPn model Henry's law constants and Fick's law coefficient of diffusion in air and pure water are shown in Table 1. In our model, we used a weighted average by volume fraction for Henry's constant and the diffusion coefficient of air in water, $H^{cc} = 1.85 \times 10^{-2}$ and $D_{air,aq} = 2.06 \times 10^{-9}$ m^2 s^{-1}, respectively. Fresh (i.e., non-shrunken, non-dried) pit membranes have cellulose fibers with no lignin and an estimated pore volume fraction of 80%, and we therefore assumed that 80% of wet pit membranes were water (Zhang et al. 2020). The conventional method of dealing with a mixture of solids and

Downloaded from https://academic.oup.com/treephys/article/43/1/88/6682843 by BIBLIOTECA CENTRAL UNIV ESTADUAL CAMPINAS user on 06 February 2025

Table 1. Henry's law constants (H^{cc}), diffusion coefficients in water ($D_{g,aq}$) and air ($D_{g,air}$), and gas concentration in water (C_{aq}) and air (C_{air}). RT = 24.8 l bar mol^{-1}, 1.013 bar = 1 atm. Avg = weighted average = sum of %air × $D_{g,aq}$ (or H^{cc}). If Ar is ignored, the weighted averages are slightly different.

Gas	$D_{g,aq}$ (m^2 s^{-1})	$D_{g,air}$ (m^2 s^{-1})	H^{cc} (C_{aq}/C_{air})	C_{aq} (mM)	C_{air} (mM)	Air (%)
Ar	2.00E-09	7.03E-05	3.43E-02	1.40E-02	0.41	1
O_2	1.88E-09	1.58E-05	3.18E-02	2.60E-01	8.17	20
N_2	2.10E-09	1.76E-05	1.49E-02	4.81E-01	32.27	79
Avg	2.06E-09		1.85E-02			

water is to reduce the diffusion coefficient by the percentage of space that is water: 80% (Einstein 1905). The rate of oxygen diffusion in lignified wood of several species has been found to be one to two orders of magnitude less than that in pure water (Sorz and Hietz 2006), so the value for radial diffusion should be reduced accordingly. The coefficient of diffusion of gases in air is four orders of magnitude larger than that in water, and in embolized vessels, the mass flow of gases can accelerate pressure equilibrium even more.

The UPPn model The UPPn model used in this study was programmed and solved in an Excel spreadsheet (see Table S1, with a description in Note S1, both available as Supplementary data at *Tree Physiology* Online). The Excel spreadsheet can be created with all equations embedded into cells and solved in a printed mathematical format. The Excel spreadsheet also has most of the intermediate and all of the final calculation results presented automatically in graphical format. Hence, only the essential features of the model are introduced below.

In UPPn, we modeled for the two slowest processes: (i) axial gas diffusion, rate-limited by diffusion across pit membranes and (ii) radial gas diffusion in concentric rings surrounding a single, embolized vessel. The radial path length and volume were adjusted in each calculation so that all non-embolized wood volume including non-embolized vessels was divided equally between all embolized vessels. Hence, if a model stem had V_s volume of non-embolized space (including conduit and non-conduit volume) and a count of N_e embolized vessels each of volume V_v, then each embolized vessel was assumed to be surrounded by V_s/N_e–V_v of non-embolized wood volume. Therefore, the water-saturated wood volume surrounding a unit embolized vessel changed with percent embolized vessels. As shown in Figure 2a, the unit pipe consisted of a cut-open vessel (left; colored gray) and one or more intact vessels that were not cut open (right; colored blue). Every cut-open vessel on the left was embolized and hence had the minimum amount of water-saturated wood in the outside radius (white). Assuming 25% embolism in Figure 2a, the shell (i.e., the water-saturated woody tissue volume) on the right side was about twice the diameter and four times the volume as on the left side. As the percentage of embolized vessels (PEV) varied, the ratio of water-saturated wood to embolized vessel diameter changed accordingly (Figure 2b).

The UPPn model provided an adequate resolution of the time course of pressure changes in intact vessels after a partial vacuum is drawn on all cut-open vessels. Because stem samples prepared for pneumatic measurements are cut in the air and the cut-open vessels become quickly embolized, they function as an extension of the discharge tubing (Figure 1). We assumed that only mature functional vessels were capable of forming embolisms. Therefore, living immature vessels, living fibers, parenchyma, cambium and living bark cells had no embolism. Hence, unit pipes near the boundary between mature and developing vessels would also receive some gas by diffusion through the water-saturated wood volume, cambium layer and living phloem in bark.

Conventionally, pneumatron data were used to compute the ratio of gas discharge after a fixed time of 15–30 s. Empirically, the amount of gas discharged into a fixed volume V_o caused a pressure increase by ΔP. The pressure discharge was the least, ΔP_{min}, at the start of an experiment and greatest, ΔP_{max}, at the end. A dimensionless value was calculated that correlated with the percentage embolism:

$$P_{AD,i} = \frac{\Delta P_i - \Delta P_{min}}{\Delta P_{max} - \Delta P_{min}} \quad (4)$$

where $P_{AD,i}$ was the *i*th percentage gas discharge, but should be close to percentage of embolized intact vessels (PEV) as demonstrated later in this paper.

The same relative discharge is calculated for ideal gases whether one uses pressure, concentration, or moles of gas in Eq. (4). The assumption is that $P_{AD,i}$ is closely related to PEV, which could equally be percent embolized vessel volume or percent loss of hydraulic conductance, PLC, in a unit pipe model. The purpose of these models is to investigate how the theoretically computed $P_{AD,i}$ (=PEV_{Pn}) relates to PEV values. In the UPPn model, all vessel diameters are equal. When there is a range of vessel diameters (d_v), and if some of the diameters would be more vulnerable than others, then the percent vessel volume is proportional to d_v^2, but the conductance is proportional to d_v^4

Downloaded from https://academic.oup.com/treephys/article/43/1/88/6682843 by BIBLIOTECA CENTRAL UNIV ESTADUAL CAMPINAS user on 06 February 2025

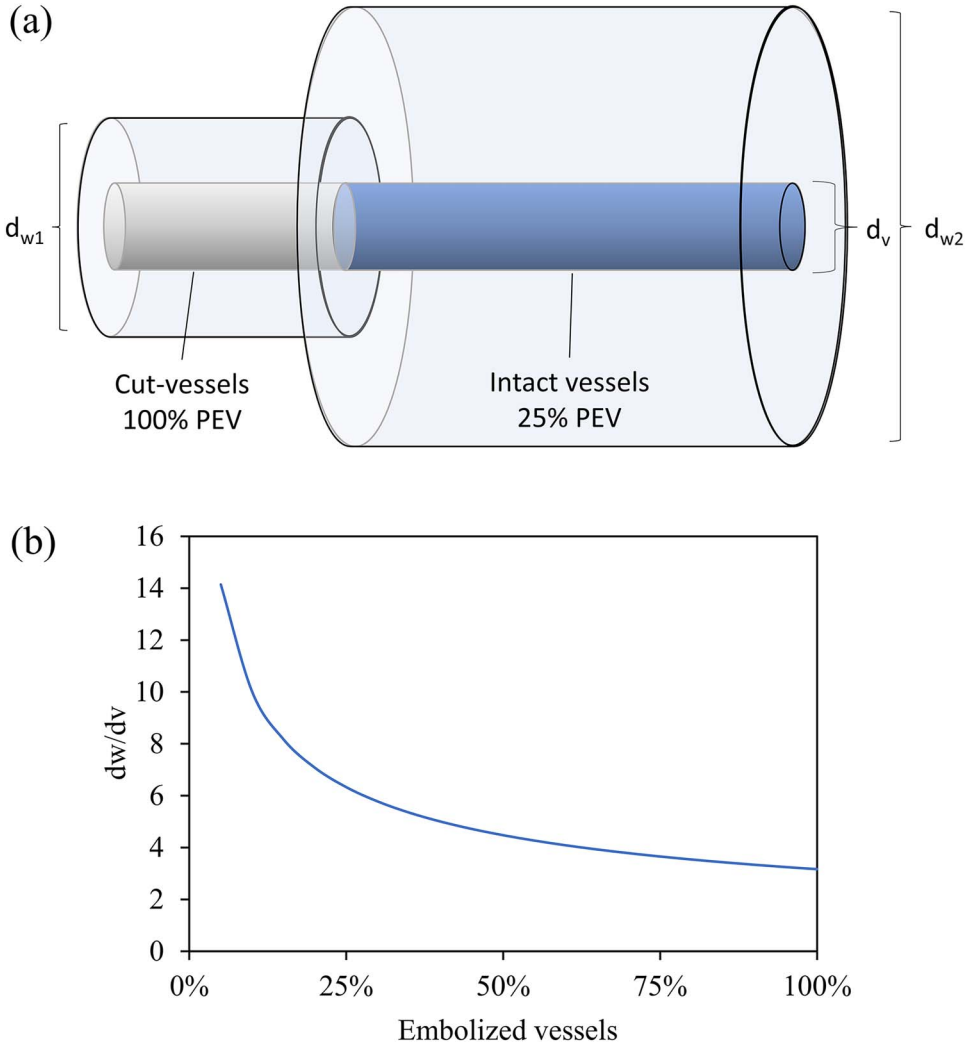

Figure 2. (a) Representative figure of the UPPn model showing a cut-open vessel and an intact, non-embolized vessel with a given diameter (d_v), a shell surrounding the cut-open vessel (d_{w1}) and a shell around the intact, non-embolized vessel (d_{w2}). (b) The ratio of the shell (d_w) to vessel diameter (d_v) versus percentage of embolized vessels (PEV). The diameter of a water-saturated shell is scaled so that all wood tissue of the shell is shared equally by the embolized unit pipes. Thus, if PEV is <100% in a region of wood, then the vessels that are embolized will share a higher shell diameter. Considering the fraction of wood area that is vessel lumina (α_x), vessel diameter (d_v) and wood diameter (d_w) in the UPPn model, the ratio d_w/d_v is given by $(\alpha_x \text{ PEV}/100\%)^{0.5}$, as shown in (b).

. We used the P_{AD} symbol for experimental values, PEV_{Pn} for theoretical values, and PEV for the actual value postulated in a stem.

We refer to the Supplementary Information for details of how the radial and axial diffusion coefficients through wood tissue were calculated (see Note S2 available as Supplementary data at *Tree Physiology* Online).

Results

Pressure dynamics in a vessel series over a 150-s period

First, we considered the case for 50% of intact vessels embolized. A UPPn model simulation of the temporal dynamics of the axial pressures in 10 vessels connected axially is shown in Figure 3. The only parameter measured by the pneumatron is the pressure in the cut-open vessels (blue line, labeled 'P_n') computed from the concentration (n/V) by the ideal gas law $P = (n/V)$RT. The pressure in the first intact, embolized vessel started out at atmospheric pressure. It could be seen that, in the first 15 s, almost no change in pressure was registered beyond the fifth vessel in series, suggesting that the pneumatron could detect the pneumatic influence of only the first few vessels in the axial chain of embolized vessels if readings were taken in <15 s as is normally done in recent pneumatic experiments.

Most of the extracted gas came from the embolized vessels rather than from the aqueous phase surrounding the vessels. After 15 s, the total gas drawn into the volume space connected to the pressure transducer (i.e., the discharge tube) came from the embolized vessel space, with a small proportion from the aqueous phase surrounding the embolized vessel. Based on

Downloaded from https://academic.oup.com/treephys/article/43/1/88/6682843 by BIBLIOTECA CENTRAL UNIV ESTADUAL CAMPINAS user on 06 February 2025

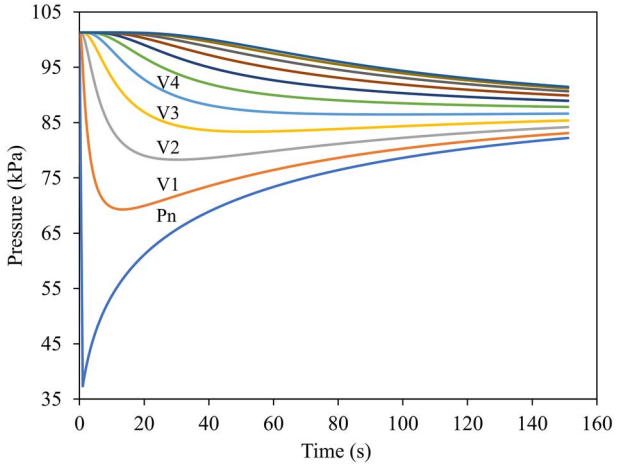

Figure 3. Simulated absolute pressures according to the UPPn model measured by the pressure transducer (blue, P_n) and as computed in the intact, embolized vessel. The *x*-axis is time; in the first second the vacuum is applied. All vessels start out at full atmospheric pressure. In the first 15 s after drawing a partial vacuum, almost no change is detected in the seventh vessel down the chain. The pressure transducer is in pressure equilibrium with the cut vessels. Vessel number is indicated above each line where space permits.

Fick's law of diffusion, the total amount of gas extracted was 1.53×10^{-9} moles, of which 91% came from the embolized space, and only 9% from the aqueous phase. Even after 150 s, the percentages of gas extracted from the gas and liquid phases were 76% and 24%, respectively. Thus, although the UPPn model slightly underestimated the rate of pressurization of vessels near the surface of the stem, radial diffusion was much slower than axial diffusion. This amount of error (i.e., 9%) was acceptable over the time domain of the model (typically 15 s).

Each solution depended on the parameters shown in Table 2 and the assumed (input) PEV. In the solution above, the model assumed 50% embolism. Hence, the radius of the external tissue was minimum in the cut-open vessels and larger in the 50% embolized zone. The radial gas concentrations in the six concentric rings of water-filled tissues to the right of the cut-open vessels were computed (Figure 4). For all concentric rings of all vessels, gas concentrations continuously decreased. The only exception was the first two rings in the first vessel; in those rings the concentration of gas reached a minimum value at 20 and 80 s, and then began to rise again (Figure 4a), which was a consequence of the nature of the simulation. The concentrations of gas in the concentric rings of intact vessels changed less than in those of the cut-open vessels. After 20 s, the gas concentrations in the rings started to increase in cut-open vessels because of air entry from vessels further down the chain. The third to sixth order vessels along the axis showed much smaller changes in dissolved gas concentration over the same 150 s than the first two vessels (Figure 4b and c, and Table S1 available as Supplementary data at *Tree Physiology* Online). Thus, even if there were many embolized vessels in an axial vessel chain, the amount of gas extracted in the first 15 s of the extraction process came mostly from the first two intact vessels.

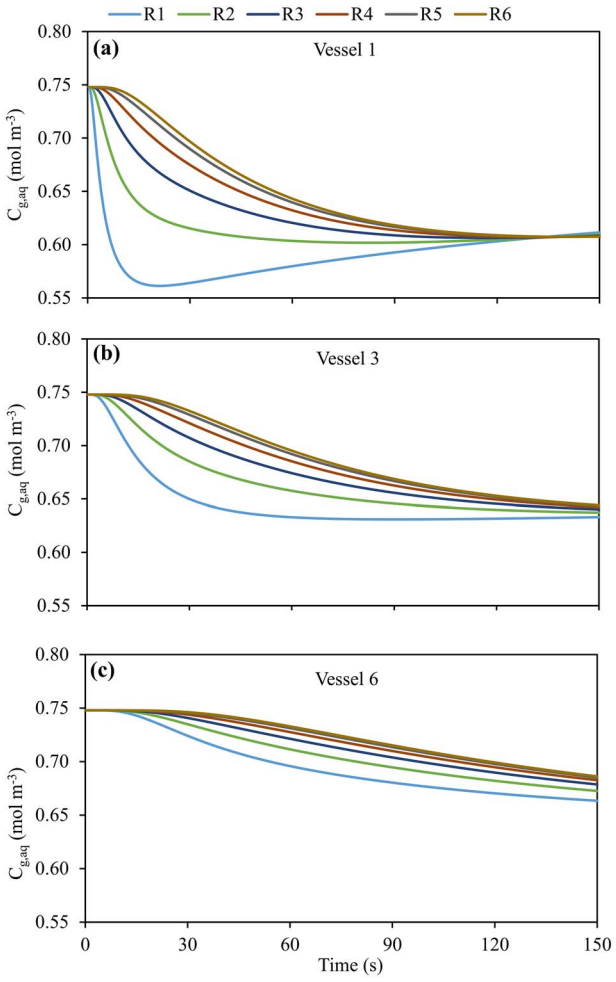

Figure 4. (a) Temporal dynamics of the axial concentrations of air in the aqueous phase of water-filled walls and wood fiber cells when 50% of the vessels are embolized. Each colored line equals the concentration of gas in water in a concentric ring of wood around the vessel. In the legend, R1, means the ring nearest the first vessel, R2, means the second ring from the vessel, etc. (b and c) Same as (a) except curves apply to the third and sixth vessel in series, respectively.

Pressure kinetics with zero embolism (P_{min})

In this case, the pneumatic model solved for a cut-open vessel that was half the mean vessel length. There was no axial draw of gas because all axial intact vessels were water filled. Therefore, we considered only the exchange of gas from water-filled wood radially adjacent to the cut-open unit pipe. In the Excel spreadsheet (see Table S1 available as Supplementary data at *Tree Physiology* Online), this was easily programmed by changing a Boolean variable (cell L44) from false to true, which indicated that the spreadsheet did not consider axial flow from vessels distal to the cut-open vessels because there were no embolized, intact vessels to allow axial flow. The spreadsheet

Downloaded from https://academic.oup.com/treephys/article/43/1/88/6682843 by BIBLIOTECA CENTRAL UNIV ESTADUAL CAMPINAS user on 06 February 2025

Table 2. Values that must be entered in the UPPn model Excel spreadsheet. The non-bold values are entered by the user; the **bold** values are calculated by Excel.

Abbreviation	Value	Units	Definition
H^{cc}	1.85E-02		Henry's law constant (weighted average for N_2 and O_2)
$C_{g,air}$	4.088E+01	mol m^{-3}	Air concentration at atmospheric pressure (saturation value)
D_{gw}	5.00E-11	m^2 s^{-1}	Diffusion coefficient of gas in wet wood (for radial diffusion)
D_g	1.65E-09	m^2 s^{-1}	Diffusion coefficient of gas in wet pit membrane
d_v	4.00E-05	m	Mean vessel diameter, diameter shared when overlapping
L_v	**6.20E-02**	m	Mean vessel length (this is computed, but can be entered manually): $2 \times 10^5 d_v^{1.48}$
$0.5L_v$	**3.10E-02**	m	Cut-open vessel length
f_v	7.5	%	Fraction of vessel wall surface in common between vessels
a_x	**10.0**	%	Fraction of vessel lumen in stem cross section
$V_v/2$	**3.89E-11**	m^3	Volume of cut-open vessel
K_{pff}	0.5	%	Fraction of the intervessel pit field that is pit membrane
d_m	5.00E-07	m	Pit membrane thickness
A_p	**2.92E-07**	m^2	Total pit membrane surface area
V_{t+v1}	**2.05E-06**	m^3	volume of V_{t+v1}
Vv	**7.79E-11**	m^3	Volume of one vessel $V_v = \pi(d_v/2)^2 L_v$
V_{cov}	**5.47E-07**	m^3	Volume of all cut-open vessels $=0.5\ V_v N_v$
d_t	0.05	s	The time step in the simulation
V_t	1.50E-06	m^3	external tubing, V_t, 1.5 ml tube
d_w	0.015	m	Diameter of wood in stem
N_v	**1.41E+04**		Number of vessels $= a_x(0.015/d_v)^2$
N_{ve}	**variable**		Number of vessels embolized to right = PEV N_v
V_{t+v}	**2.05E-06**	m^3	Volume of cut-open vessels plus tubing

Notes: The first two values are physical constants that should not be altered. The next two values are diffusion coefficients for gases in lignified wood (D_{gw}) (Sorz and Hietz 2006) and pit membranes (D_g). The estimated D_g (Table 1) was reduced by 20% to allow for the pit membrane having solid cellulose fibers occupying approximately 20% of the volume $= 0.8 \times 2.06 \times 10^{-9}$. The following three values are all available from the literature (Zanne et al. 2010, Morris et al. 2016) or can be measured anatomically: (i) the fraction of vessel walls in common between vessels (Sperry et al. 2005, 2006), (ii) the percentage of stem cross section that is vessel and (iii) vessel diameter. The fraction of pits in the pit field varies over a narrow range from 0.4 to 0.6 (Lens et al. 2011, Scholz et al. 2013). The thickness of pit membranes varies from 0.2 to 1.2 μm (Li et al. 2016, Kaack et al. 2019). Finally, d_t is a step time interval that must be small enough for the computational results to be stable. This is determined by trial and error and changes with the impact of all the other parameters. The last two values are the volume of tubing connected to the pressure transducer and the diameter of the wood. These values are used to compute the number of vessels and the external volume per vessel, because the UPPn needs to scale the volume where pressure is measured in a single vessel series (unit pipe). Vessel length, L_v, is computed, but has no influence on the model results. However, it is important for experimental design because excised shoots must be cut several times longer than the vessels contained in shoot segments. Not shown in this table, but calculated in the Excel spreadsheet, are one value of axial conductance (k_a) for axial diffusion of air through pits [Eq. (S12), Note S2 available as Supplementary data at *Tree Physiology* Online] and six values of radial conductance (k_r) for the radial diffusion of air through the six radial shells [Eq. (S7), Note S2 available as Supplementary data at *Tree Physiology* Online] around each vessel; k_a and k_r have units equal to m^3 s^{-1}.

for this simple case computed a very small change in moles of gas in the discharge chamber connected to the pressure transducer after turning off the pump: 7.45×10^{-11} mol in 15 s and 1.54×10^{-10} mol in 150 s after turning off the pump. Theoretically, this should be the same as setting PEV (cell O39) to zero, but this would cause the programed Excel sheet to crash because this value was used to compute the radial distance of water-filled tissue between equally spaced embolized vessels.

Pneumatron absolute pressure curves and PEV_{Pn} curves versus model input PEV

The impact of the extractable gas (model output) as the input PEV increased from zero (cell L44 = true) to 100% (cell L44 = false, cell O39 set to the desired PEV) is shown in Figure 5a. Minimal change in pressure ΔP_{min} occurred at 0% PEV input, and the maximum ΔP_{max} occurred when 100% PEV was inputted. Readers should remember that, in the UPPn model, an increase in PEV was equivalent to a decrease in the radius of water-saturated shell around the embolized vessel. The conventional method of estimating the PEV in real experimental studies was to pick some time interval (e.g., 15 s) and then compute PEV_{Pn} following Eq. (4). Taking the ΔP_i measurements at 15 s for every curve in Figure 5a produced the results shown in Figure 5b. The relationship was linear, with a maximum deviation of approximately 8% at the 50% PEV input value. It could be seen that the time interval for ΔP_i influenced the closeness of fit of PEV_{Pn} to PEV.

Sensitivity analysis

The rate-limiting steps for gas movement occurred when gas was forced to move through the water by diffusion. When there was no embolism at all in intact vessels, the gas extraction was

Downloaded from https://academic.oup.com/treephys/article/43/1/88/6682843 by BIBLIOTECA CENTRAL UNIV ESTADUAL CAMPINAS user on 06 February 2025

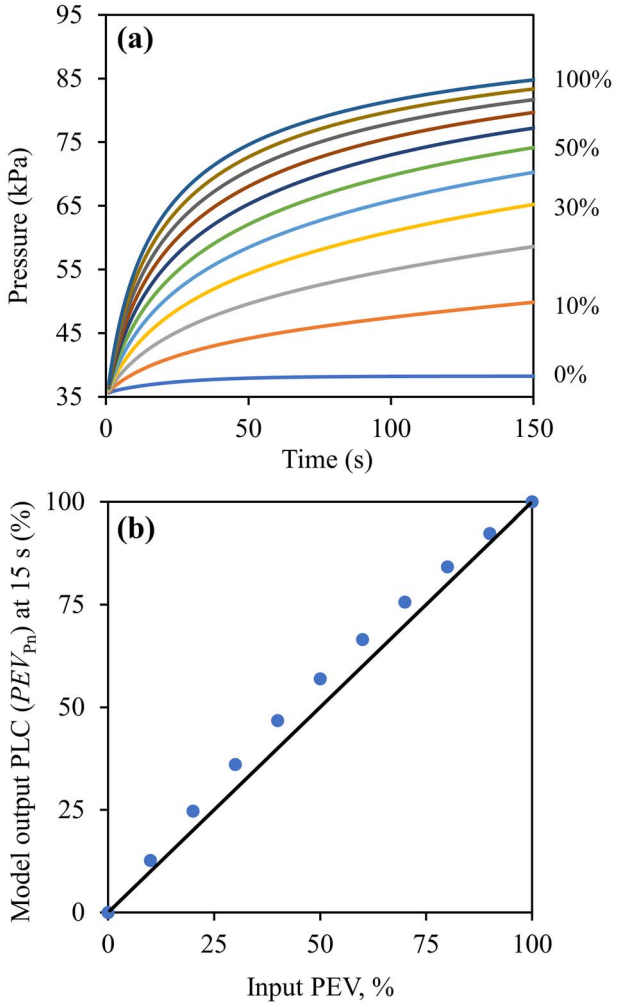

Figure 5. (a) Temporal dynamics of simulated pressure output (kPa) at the pressure transducer with varying percentage of embolized vessels (PEV). In the simulation, the partial vacuum is drawn in the 1 s before time 0 on the *x*-axis. The different curves give the gas pressure change when varying the percentage of embolism in the stem (shown on the right). (b) A plot of simulated PEV_{Pn} from the model versus the input PEV. The points are taken from the curves in (a) at $t = 15$ s using Eq. (4). The black line represents the 1:1 line.

limited to what came out of solution from the surrounding water radially connected to the cut-open vessel [ΔP_{min} in Eq. (4)]. When vessels were all embolized, the maximum air extraction occurred from the embolized vessels plus the extraction from the water-filled tissue surrounding the vessels [ΔP_{max} in Eq. (4)].

The rate of gas extraction from intact vessels was faster than that from surrounding water because the diffusional path length is equal to the intervessel pit membrane thickness (0.2–1.2 μm), whereas radial diffusion was over a distance of 60–150 times the typical pit membrane path length (30–75 μm depending on vessel diameter) when the volume fraction of the vessel occupied 10% of the cross-sectional area of the wood (Zanne et al. 2010, Morris et al. 2016).

The mass flow rate of gas down the length of the vessel lumen was much more efficient than that of diffusion. The maximum gas flow down the axis of the vessel occurred in the first intact vessel adjacent to the cut-open vessel immediately after the vacuum was drawn. The theoretical pressure drop needed to maintain flow down the entire vessel length was calculated to be smaller than 10^{-3} Pa out of nearly 10^5 Pa initial pressure; hence, pressure gradients through the length of intact vessels could be ignored compared with the pressure difference across wet intervessel pit membranes.

In most simulations, at least 90% of gas was extracted from the vessels during the first 15 s. Vessel length had no impact on the fraction of extracted gas because increasing vessel length increased the moles of air in the embolized vessel and increased in equal proportion to the moles of air in the surrounding water-saturated tissue. In contrast, increasing the vessel diameter increased the percentage of gas extracted from the embolized vessels, even though the volume of water-saturated shells dramatically increased with the vessel diameter (see Figure S1 available as Supplementary data at *Tree Physiology* Online). Nevertheless, a gas extraction percentage of 85–95% illustrated the use of pneumatic experiments to estimate embolism resistance in angiosperms. These percentages were computed for an analysis period of 15 s, and a 50% embolism scenario. The agreement improved slightly as the input PEV decreased. For example, for a 40-μm diameter vessel, the percentage gas extraction increased from 90.3 to 91.0% at 100% PEV input. The decision about the appropriate time interval for analysis of real experiments versus simulated data was demonstrated with one experimental example.

So far, we have presented results from the UPPn model using only one set of input parameters, as shown in Table 2. These are the default values available to readers who wish to download the Excel file. The only factor that changed was the input PEV value. We therefore examined how much the model output changed when other input values were selected that might have influenced the UPPn model. Based on quantitative anatomy, the values in Table 2 cannot be independently varied and be expected to be meaningful (Sperry et al. 2005, Hacke et al. 2006, Sperry et al. 2006). For example, vessel length (L_v) was found to scale with vessel diameter squared, and L_v (cm) $\cong 2.6 \times 10^{-2}\ D_v^{1.48}$ (μm) (Liu et al. 2018); converting both sides to meters yielded $L_v = 2.00 \times 10^5\ D_v^{1.48}$. In addition, end wall resistivity in pits was assumed to scale with lumen resistivity with a slope near one. The initial UPPn model took these factors into account when default values were loaded in Table 2 (copied from the Excel file available for download).

Influence of axial conductance (k_a) on pneumatron results

The axial conductance (k_a) used in the calculations was a diffusional conductance for gas through pit membranes, whereas the statement about hydraulic resistivities being nearly equal

Downloaded from https://academic.oup.com/treephys/article/43/1/88/6682843 by BIBLIOTECA CENTRAL UNIV ESTADUAL CAMPINAS user on 06 February 2025

refers to the resistance to water flow per unit length of wood. Pit membranes were typically 0.3–0.5 μm thick (range about 0.2–1.2 μm) compared with vessel lumen lengths that are 10^4 to 10^6 times longer (5–50 cm or more). The UPPn model considered the rate-limiting step of the diffusion of gases through the water-filled spaces of pits that were approximately 80% water by volume in fresh pit membranes (Zhang et al. 2020).

The model predicted that after 15 s, more than 90% of the gases drawn into the tubing connected to the pressure transducer came from axial gas extracted from embolized vessels, and less than 10% came from gases dissolved in the water of fully hydrated tissue surrounding the vessel. Therefore, we started with the assumption that factors influencing k_a dominated the gas-extraction process. There were four constants in Eq. (S12) (see Note S2 available as Supplementary data at *Tree Physiology* Online). The value of Δt was the time step used for the iterative solution of the equations, and we picked a small enough value so that the solution was stable. The two most variable constants were the pit membrane area between adjacent vessels (A_p) and the thickness of the pit membrane (d_m). The value of A_p seemed to range over two orders of magnitude from 3×10^{-7} to 3×10^{-9} m^2 (Wheeler et al. 2005, Hacke et al. 2006, Jansen et al. 2011, Lens et al. 2011, Scholz et al. 2013) and was suggested to be negatively correlated with vulnerability to embolism (Wheeler et al. 2005, Hacke et al. 2006), but see Kaack et al. (2021). Values of d_m could range from 0.2 to 1.2 μm (Li et al. 2016). Since k_a was a function of the ratio of A_p/d_m, it seemed reasonable to explore how this ratio changed over a factor of 10 from 2 to 0.2 m, and this was accomplished by changing k_a from 5×10^{-12} to 5×10^{-11}. The results, ΔP vs k_a, are plotted in Figure 6a over a slightly larger range of k_a values. Figure 6b displays a plot of the simulated value, PEV_{Pn}, which is the model output value when the input value was 50% PEV while varying k_a.

The simulation demonstrated that changing k_a over likely values in plants increased the model-computed values of ΔP_{max} and ΔP_{50} when the real input value was 50% (Figure 6a). ΔP_{min} was unaffected by k_a because there were no embolized vessels to deliver gases (Figure 6a). The computed tension at PEV_{50} compared with PEV_{Pn} from the pneumatron was in error of 5–19% from the PEV_{50} as k_a increased from 5×10^{-12} to 5×10^{-11} at measuring cycle of 7.5 s (Figure 6b, blue line), and hence, based on our current model, it appeared that the pneumatron may overestimate the tension of PEV_{50}. However, such overestimation of PEV_{50} would have a low impact on T_{50} (less than 0.11 MPa), as shown in a typical VC (Figure 6c).

The impact of radial diffusion of gases on pneumatron results

Figure 6a shows that the radial diffusion had little impact on ΔP_{max} and ΔP_{50} (compare solid lines to dashed lines), and

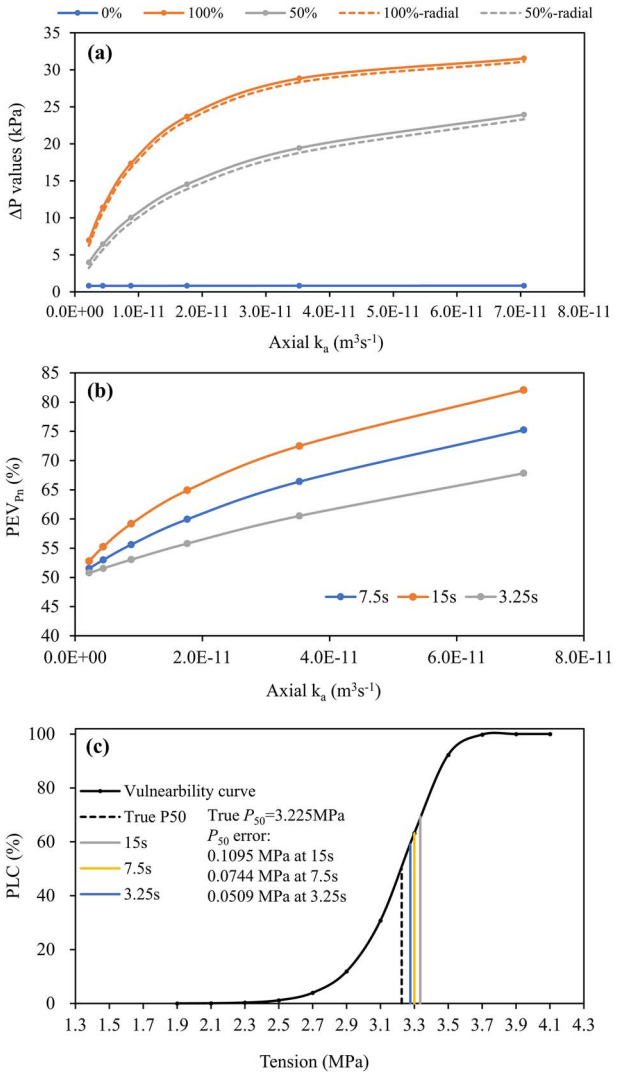

Figure 6. Theoretical impact of axial conductance of pit membranes to air diffusion (k_a) on the computed change in gas pressure (ΔP). (a) The computed pressure values, ΔP, after 15 s for 0% (ΔP_{min}), 50% (ΔP_{50}) and 100% (ΔP_{max}) embolism as affected by k_a. The dashed lines give the values ΔP when radial diffusion is set to zero, the solid lines give the complete model. (b) The pneumatic value of PEV_{Pn}, when PEV = 50%, as affected by k_a. (c) The maximum likely error in determining the tension at 50% PEV (T_{50}) is shown on a typical vulnerability curve, assuming an overestimation of 17% in PEV_{50}. In order to increase the precision of results, the time step for these simulations was reduced from 0.05 to 0.01 s.

on the computed value of the PEV_{Pn} percentage value by less than 0.03% at 15-s interval. Starting with the default values (5×10^{-11} m^2 s^{-1}, Table 2), the percentage of gas extracted from radial pathways was 5.8% of the total amount of gas extracted. Decreasing the diffusion coefficient by a factor of two decreased this percentage to 3.5%, and increasing the diffusion coefficient by a factor of two increased the radial extraction to 8.3%. Hence, our sensitivity analysis suggested that PEV may be a robust estimate of embolism resistance.

Downloaded from https://academic.oup.com/treephys/article/43/1/88/6682843 by BIBLIOTECA CENTRAL UNIV ESTADUAL CAMPINAS user on 06 February 2025

Table 3. Computations of slopes versus the traditional ΔP from theoretical outputs using timing similar to experimental data in Figure 9 for *Eucalyptus*. The number of vessels in series (in the first column) connected axially was varied from 1 to 10. The 3-s interval used for these calculations was from $t = 3$ to 6 s. The ΔP_{50} is for 50% PEV_{Pn}. Slopes refer to the rate of change of pneumatron pressure versus time for 3 s, dP/d_t.

#Vessels	ΔTime 3 s, ΔP (kPa)			PEV_{Pn}	Slope (kPa s^{-1}), 3 s			PEV_{Pn}
	ΔP_{min}	ΔP_{50}	ΔP_{max}		m_{min}	m_{50}	m_{max}	
1	0.3022	3.3290	5.8110	54.94%	0.1002	1.1071	1.9312	54.99%
2	0.3022	3.5080	6.1442	54.88%	0.1002	1.1665	2.0421	54.91%
3	0.3022	3.5100	6.1481	54.87%	0.1002	1.1672	2.0433	54.91%
10	0.3022	3.5100	6.1481	54.87%	0.1002	1.1672	2.0433	54.91%

Discussion

The UPPn model demonstrates that embolism in intact vessels can be accurately measured with the pneumatic method. The main reason why this method based on gas diffusion kinetics works is that gas flow via pit membranes is about 100 times faster than radial flow across cell walls (compare D_g and D_{gw} values in Table 2). The model also showed that the first 15 s of gas extraction are the most important ones to estimate embolism, while longer extraction times result in slightly higher levels of gas from the aqueous phase.

Pneumatic measurements quantify embolism directly and accurately based on fast gas movement between intervessel pit membranes

When a vessel was embolized, gas could diffuse from the hydrated tissue immediately adjacent to the embolized vessel. Pulling a partial vacuum at the end of a xylem segment results in axial diffusion of gases from the nearby embolized vessels, which were initially at atmospheric pressure. Then, as the intact vessel pressure drops, there is a tendency for gases to diffuse from the surrounding tissue. The UPPn model demonstrated that the axial rate of diffusion is faster than the radial rate. This is the consequence of two factors: (i) the distance of diffusion is about 100 times greater than the axial diffusion distance in wet pit membranes; and (ii) the coefficient of diffusion is up to two orders of magnitude less in water-saturated wood (Sorz and Hietz 2006) compared with that in pure water.

The values of the O_2 diffusion coefficient measured in water-saturated wood are 1×10^{-11} to 2×10^{-10} m^2 s^{-1}, which are lower than that in pure water (2×10^{-9} m^2 s^{-1}). The default value used for our calculations is 5×10^{-11} m^2 s^{-1}. We use this low value because the wood samples studied by Sorz and Hietz (2006) were from stems that still had some embolism (5–20% gas volume). Exactly where this gas was located was not specified by the authors, but the range of gas contents was close to the percentage of stem volume that contained vessel lumina in most woody species (5–20%) (Zanne et al. 2010, Morris et al. 2016). Increasing the gas content by another 10% typically causes a 10-fold increase in the diffusion coefficient. This is because the pathway of gas movement involves water and gas in parallel and series pathways, and the coefficient of diffusion of gas in gaseous medium is 10^4 times larger than that in water (Table 1). Hence, the 5×10^{-11} m^2 s^{-1} value we use in our model may still have been too large and was already five times the minimum value (Sorz and Hietz 2006). Yet, this value provides a conservative approach, so that the amount of gas extracted from the aqueous phase was more likely overestimated than underestimated.

The initial rate of gas extraction is the best predictor of embolism

The highest overall agreement between pneumatic VCs and a flow-centrifuge method was found after 15 s of gas extraction (Paligi et al. 2021). However, our model indicates we can do better. We did a statistical analysis of the uncertainties in measuring time, δt_e, and in gas extraction, δP_e, and this analysis showed that a measuring interval of as few as seven pressure measurements over a 3-s time interval will yield accurate values of pneumatron PLCs (Table 3).

Using the UPPn model, the PEV_{Pn} values give the same result from analysis of slopes versus pressure differences [Eq. (4) and Table 3]. While varying the number of vessels connected axially from 1 to 10, PEV_{Pn} computed from ΔP was 54.94% to 54.87% and, hence, depended slightly on the number of vessels connected. When slope, m, was used, the PEV_{Pn} was not significantly different, so it may not be necessary for future studies, but is worth confirming with more real-data examples in other species. In Table 3, the simulation suggests there is no advantage of slopes versus ΔP values. Real data of *Eucalyptus camaldulensis* (Pereira et al. 2020), which included the measuring error in P during pneumatron measurements, suggested that time intervals as short as 3 s can yield relatively noise-free curves of slopes for time intervals starting at 3–6 s from the time the pump is turned off (Figure 7). Indeed, the R^2 values are better for slopes computed over 3 s versus slopes for 7 s (3–10 s after the vacuum is drawn).

From how many vessels in series can gas be extracted?

Our model results assume that there are 10 embolized vessels in series regardless of the input PEV. As long as model output PEV_{Pn} values are computed in the first 15 s after vacuum

Downloaded from https://academic.oup.com/treephys/article/43/1/88/6682843 by BIBLIOTECA CENTRAL UNIV ESTADUAL CAMPINAS user on 06 February 2025

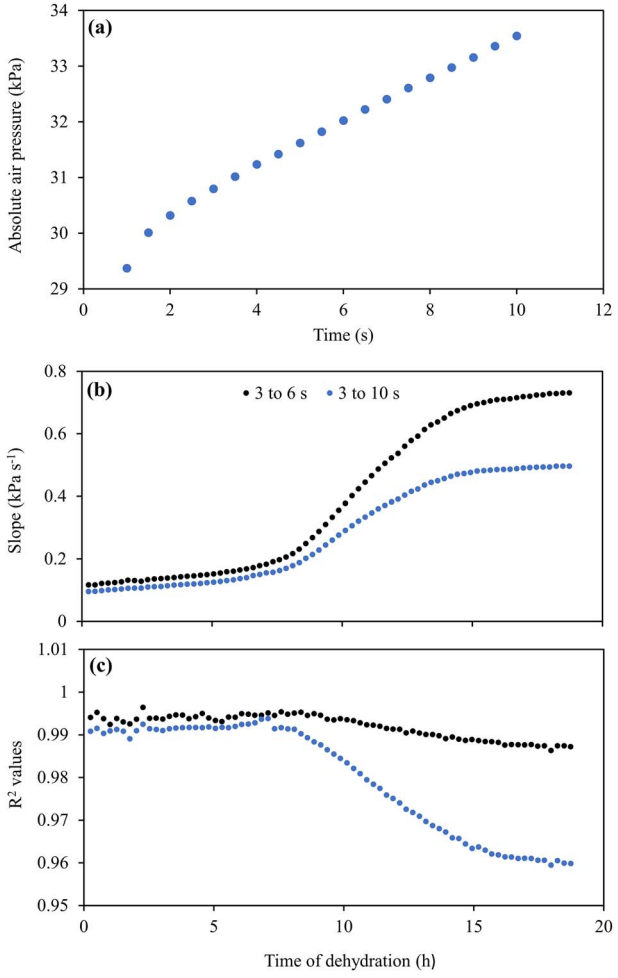

Figure 7. Analysis of experimental pneumatron data collected during the dehydration of a *Eucalyptus camaldulensis* Dehnh. Shoot with leaves (data from Pereira et al. 2020). (a) Typical change in absolute pressure with time during the early hours of shoot dehydration. (b) Slopes (dP_{Pn}/dt) calculated for 3-s (black symbols) and 7-s periods (blue symbols) as affected by the dehydration time. Slopes were calculated after the initial 3 s, when there was a more linear correlation between pressure and time, as shown in (a). (c) R^2 values of the slope values shown in (b) during dehydration time.

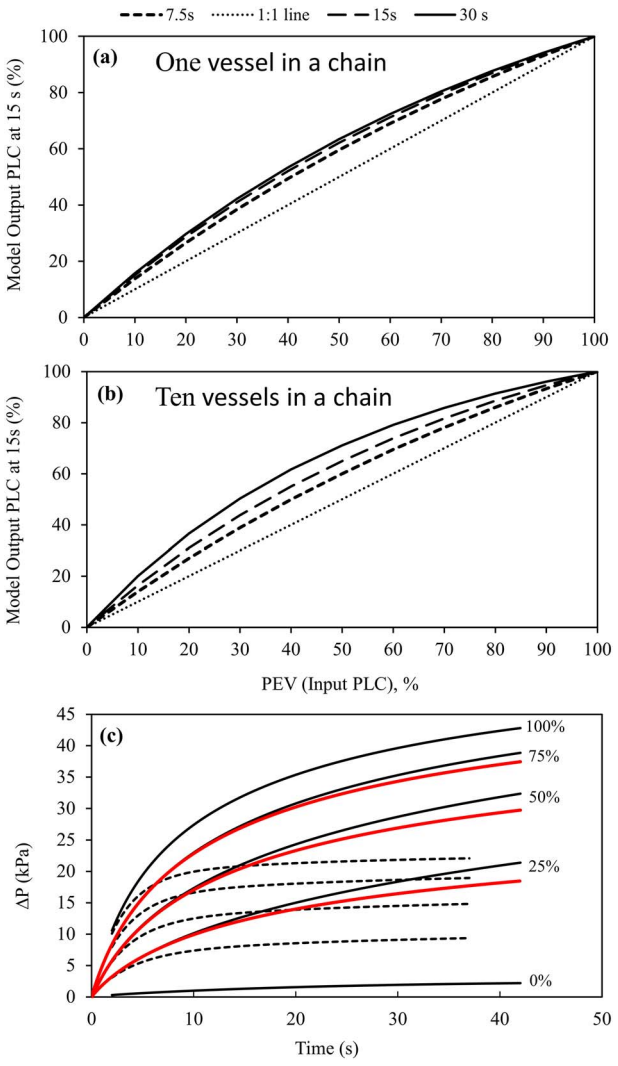

Figure 8. These figures are theoretical calculations comparing input PEV on the *x*-axis to PEV_{Pn} on the *y*-axis for two cases: (a) only one vessel in a chain regardless of PEV; and (b) always 10 vessels in a chain regardless of PEV. (c) The time course of the gas extraction values, ΔP, on the *y*-axis versus time on the *x*-axis. In (c), the dashed lines are for one vessel, black solid lines are for 10 vessels in series and the red solid lines are for three vessels in series. Dashed lines have the same PEV values as solid lines in sequence from 100% to 0%.

draw, the number of vessels in series is not very important. This can be demonstrated by looking at model output PEV_{Pn} versus input PEV for the extreme cases of 1 vessel versus 10 vessels regardless of PEV (Figure 8a and b). By allowing only one vessel to contribute to pneumatic measurements, it can be seen that the resulting deviations for sampling time intervals of 7.5, 15 and 30 s move closer together. In contrast, the deviation between input PEV and output PEV_{Pn} becomes only slightly worse for the 7.5 s sampling interval, with 59.6% for only one vessel (Figure 8a) versus 60% output PEV_{Pn} for 10 vessels (Figure 8b) for an input PEV = 50%. The reason for this is evident from the pneumatron gas kinetics (Figure 8c). With only one vessel in the model, the system equilibrates within about 15 s, i.e., the gas extraction values (ΔP values) become almost constant versus time (dashed line). But for 10 vessels in series, there are still dynamic increases in ΔP when the input PEVs are 25% or greater (solid black lines); the red lines are for 3 vessels in series.

Based on a given likelihood of embolism spread between vessels, we can estimate how many vessels in series are embolized at any given PEV. There needs to be an embolized vessel to seed the next embolism in an adjacent water-filled vessel. In many experimental situations, there are cut shoots or cut stem segments, and at each cut surface all vessels are embolized. Assume there are 14,000 vessels cut open at the cross section of a branch (see Table 2 for the equation used

Downloaded from https://academic.oup.com/treephys/article/43/1/88/6682843 by BIBLIOTECA CENTRAL UNIV ESTADUAL CAMPINAS user on 06 February 2025

to estimate this number). When the branch is dehydrated until 10% PLC has been induced in intact vessels adjacent to the cut surface, there will be 1400 embolized, intact vessels. Then, there is a 10% chance of the next vessel in the chain being embolized (= 140 vessels). At the third vessel in the chain, there will be 14 embolized vessels. By the fourth vessel in series, there will be only 1.4 vessel embolized (statistically speaking). Figure 9a is the graph showing how a 10% PLC scenario predicts the percentage of embolized vessels in a stem (y-axis) versus the number of vessels in series counting from the base on the *x*-axis. Figure 9b shows the number of embolized vessel chains on the *y*-axis versus chain length on the *x*-axis, where the chain length is defined as the number of vessels in a given chain of embolized vessels. In Figure 9b, there are 14,000 vessels in any given cross section of stem, and we plot the number of embolized chains that are of length 1–10 vessels per chain (*x*-axis). Taking the 10% PLC example above, there are 1.4 chains with four embolized vessels, there are 12.7 chains (=14–1.4) of length 3; for chain length = 2 there are 126.6 chains (=140–15.4), and so on. At the 50% PLC, the sum of the vessel chains equals 7000 chains of variable chain length from 1 to 10 embolized vessels, with 13.7 chains of length = 10 cells and 3500 chains of length = 1.

Of course, there could be other embolized vessels scattered throughout the shoot, e.g., where a leaf or branch has been injured. These formerly embolized vessels could also serve to seed new chains of vessels growing longer towards the chains growing from the cut base (Guan et al. 2021). Chains of embolized vessels from apical regions could randomly join up chains growing from the base of the excised branch. The impact of variable chain length on gas extraction can be seen in Figure 8c (black lines, red lines and dashed lines are for chain lengths of 10, 3 and 1, respectively). Embolized chains have no impact on the kinetics of gas extraction for the first 10–15 s, where the black and red lines nearly coincide. If PLC_{Pn} is calculated for gas extraction times of 7.5 s or less, the amount of gas extracted will not be influenced by the chain length of embolized vessels, because most of the gas is extracted from the most basal embolized vessels.

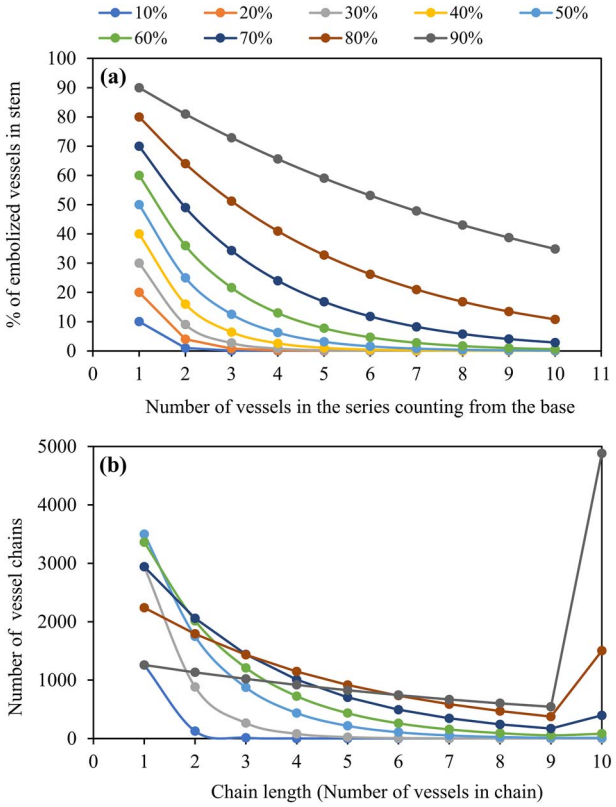

Figure 9. This graph shows the consequences of the air-seeding hypothesis on a chain of up to 10 embolized vessels. (a) The percentage of embolized vessels is shown on the *y*-axis. The *x*-axis represents the vessel count (1 = nearest the cut base of a shoot, and 10 = the 10th vessel in the axial series). Colors represent the input PLC at the first vessel. (b) The number of embolized vessel chains in a stem cross section with 14,000 vessels versus chain length = the number of embolized vessels in the chain.

Insights from a theoretical approach on plant pneumatics

Much more work on modeling of gas movement in stems seems to be merited by the results of this study. The tentative conclusion from the mathematical modeling of the biophysical process of gas movement in woody stems provides a strong justification for the pneumatic method of measuring VCs and gas kinetics.

It is important to remember that an accurate VC depends on accurate measurements of both the *y*-axis values (PLC) and the *x*-axis values (water tension) as in Figure 6c. Both methodological errors in the measurement of xylem water potential and errors in pneumatic experiments should be considered when estimating embolism resistance, while additional aspects may affect embolism spreading, such as segmentation and the vicinity to a gas source (Guan et al. 2021). For instance, incorrect estimation of the minimum and maximum amount of air discharge will result in incorrect pneumatic VCs (Chen et al. 2020, Sergent et al. 2020, Pereira et al. 2021). Users who are new to the pneumatic method should pay special attention to the fact that stable measurements of the minimum and maximum amount of gas discharge are obtained, which is easier when working with a pneumatron than when using the manual pneumatic approach. Pneumatic experiments should not stop too early before a stable plateau of maximum amount of gas discharge has been achieved (Pereira et al. 2021, Trabi et al. 2021). The importance of reference values (for maximum and minimum hydraulic conductivities) as the functional starting and ending point in VCs also applies to hydraulic VCs (Choat et al. 2010, Jansen et al. 2015).

Another potential measuring error could result from the volume of the discharge tube. If the discharge volume is too large, the measuring error of the pressure sensor will be relatively large (see Figure 4 in Jansen et al. 2020). We therefore recommend adjusting the volume of the discharge

Downloaded from https://academic.oup.com/treephys/article/43/1/88/6682843 by BIBLIOTECA CENTRAL UNIV ESTADUAL CAMPINAS user on 06 February 2025

tube by determining the maximum volume of the gas that can be extracted from a completely dehydrated sample before conducting VC measurements (Pereira et al. 2020). Stems with short vessels require low volumes connected to the pressure transducer in the pneumatron.

The comparison of the pneumatic with hydraulic and other non-hydraulic methods has provided strong agreement for a substantial number of angiosperm species and samples (see Figure S2 and Table S2 available as Supplementary data at *Tree Physiology* Online, Pereira et al. 2016, 2020, 2021, Zhang et al. 2018, Sergent et al. 2020, Guan et al. 2021, Paligi et al. 2021). This agreement is especially strong when the above-mentioned caveats are considered. Therefore, we assert tentatively that there is a good theoretical and experimental basis for applying the pneumatic method in research on plant water relations and embolism resistance. Ideally, future work should combine experimental work with the development of more precise three-dimensional models to investigate gas–liquid–solid interactions in xylem with different vessel arrangements, size distributions, and intervessel connectivity.

Supplementary data

Supplementary data for this article are available at *Tree Physiology* Online.

Data availability statement

The data supporting the findings of this study are available within the paper and supplementary files.

Conflict of interest

The authors declare that they have no conflict of interest.

Funding

This research was funded by the National Natural Science Foundation of China (31770647), the Zhejiang Provincial Natural Science Foundation of China (LY19C150007) and the German Research Foundation (DFG, Deutsche Forschungsgemeinschaft, project nrs 457287575 and 410768178). The authors acknowledge the São Paulo Research Foundation (FAPESP, Brazil) for a grant (M.T.T. and R.V.R., grant #2019/24519-1) and fellowship (L.P. and R.V.R., grant #2017/14075-3). R.V.R. is a fellow of the National Council for Scientific and Technological Development (CNPq, Brazil).

Authors' contributions

D.Y., G.P. and M.T. conceived the research plans; M.T., D.Y., G.P., L.P. and S.J. developed the model and contributed to the writing. L.P. provided experimental data for model analysis. R.V.R. and L.K. contributed to the manuscript.

References

Avila RT, Guan X, Cardoso AA, Kane CN, Batz TA, DaMatta FM, Jansen S, McAdam SAM (2022) Xylem embolism spread is largely prevented by interconduit pit membranes until the majority of conduits are gas-filled. Plant Cell Environ 45:1204–1215.

Benkert R, Zhu JJ, Zimmermann G, Türk R, Bentrup FW, Zimmermann U (1995) Long-term xylem pressure measurements in the liana *Tetrastigma voinierianum* by means of the xylem pressure probe. Planta 196:804–813.

Brodersen CR, McElrone AJ, Choat B, Lee EF, Shackel KA, Matthews MA (2013) In vivo visualizations of drought-induced embolism spread in *Vitis vinifera*. Plant Physiol 161:1820–1829.

Brodribb TJ, Bienaimé D, Marmottant P (2016*a*) Revealing catastrophic failure of leaf networks under stress. Proc Natl Acad Sci USA 113:4865–4869.

Brodribb TJ, Skelton RP, McAdam SAM, Bienaimé D, Lucani CJ, Marmottant P (2016*b*) Visual quantification of embolism reveals leaf vulnerability to hydraulic failure. New Phytol 209:1403–1409.

Chen YJ, Maenpuen P, Zhang YJ, Barai K, Katabuchi M, Gao H, Sasiwimol K, Tao LB, Zhang JL (2020) Quantifing vulnerability to embolism in tropical trees and lianas using five methods: Can discrepancies be explained by xylem structural traits? New Phytol 229:805–819.

Choat B, Drayton WM, Brodersen C, Matthews MA, Schackel KA, Wada H, McElrone AJ (2010) Measurement of vulnerability to water stress-induced cavitation in grapevine: a comparison of four techniques applied to a long-vesseled species. Plant Cell Environ 33:1502–1512.

Choat B, Badel E, Burlett R, Delzon S, Cochard H, Jansen S (2016) Non-invasive measurement of vulnerability to drought induced embolism by X-ray microtomography. Plant Physiol 170: 273–282.

Cochard H, Delzon S (2013) Hydraulic failure and repair are not routine in trees. Ann For Sci 70:659–661.

Cochard H, Damour G, Bodet C, Tharwat I, Poirier M, Améglio T (2005) Evaluation of a new centrifuge technique for rapid generation of xylem vulnerability curves. Physiol Plant 124:410–418.

Cochard H, Badel E, Herbette S, Delzon S, Choat B, Jansen S (2013) Methods for measuring plant vulnerability to cavitation: a acritical review. J Exp Bot 64:4779–4791.

Crank J (1975) The mathematics of diffusion. Oxford University Press, Oxford, UK.

Dietrich L, Delzon S, Hoch G, Kahmen A (2019) No role for xylem embolism or carbohydrate shortage in temperate trees during the severe 2015 drought. J Ecol 107:334–349.

Einstein A (1905) Investigations on the theory of Brownian motion. Ann Phys Rehabil Med 17:549–560.

Gartner BL, Moore JR, Gardiner BA (2004) Gas in stems: abundance and potential consequences for tree biomechanics. Tree Physiol 24:1239–1250.

Guan X, Pereira L, McAdam S, Cao KF, Jansen S (2021) No gas source, no problem: pre-existing embolism may affect non-pressure driven embolism spreading in angiosperm xylem by gas diffusion. Plant Cell Environ 44:1329–1345.

Guan X, Werner J, Cao KF, Pereira L, Kaack L, McAdam SAM, Jansen S (2022) Stem and leaf xylem of angiosperm species experiences minimal embolism in temperate forests during two consecutive summers with moderate drought. Plant Biol. https://doi.org/10.1111/plb.13384.

Hacke UG, Sperry JS, Wheeler JK, Castro L (2006) Scaling of angiosperm xylem structure with safety and efficiency. Tree Physiol 26:689–701.

Jansen S, Gortan E, Lens F, Lo Gullo MA, Salleo S, Scholz A, Stein A, Trifilò P, Nardini A (2011) Do quantitative vessel and pit characters

Downloaded from https://academic.oup.com/treephys/article/43/1/88/6682843 by BIBLIOTECA CENTRAL UNIV ESTADUAL CAMPINAS user on 06 February 2025

account for ion-mediated changes in the hydraulic conductance of angiosperm xylem? New Phytol 189:218–228.
Jansen S, Schuldt B, Choat B (2015) Current controversies and challenges in applying plant hydraulic techniques. New Phytol 205:961–964.
Jansen S, Guan X, Kaack L, Trabi CL, Miranda MT, Ribeiro RV, Pereira L (2020) The pneumatron estimates xylem embolism resistance in angiosperms based on gas diffusion kinetics: a mini-review. Acta Horticult 1300:193–200.
Jansen S, Bittencourt P, Pereira L, Schenk HJ, Kunert N (2022) A crucial phase in plants - it's a gas, gas, gas! New Phytol 233:1556–1559.
Kaack L, Altaner CM, Carmesin C et al. (2019) Function and three dimensional structure of intervessel pit membranes in angiosperm xylem: a review. IAWA J 40:673–702.
Kaack L, Weber M, Isasa E et al. (2021) Pore constrictions in intervessel pit membranes provide a mechanistic explanation for xylem embolism resistance in angiosperms. New Phytol 230:1829–1843.
Knipfer T, Brodersen CR, Zedan A, Kluepfel DA, McElrone AJ (2015) Patterns of drought-induced embolism formation and spread in living walnut saplings visualized using X-ray microtomography. Tree Physiol 35:744–755.
Lamarque LJ, Corso D, Torres-Ruiz JM et al. (2018) An inconvenient truth about xylem resistance to embolism in the model species for refilling *Laurus nobilis* L. Ann For Sci 75:88. https://doi.org/10.1007/s13595-018-0768-9.
Lens F, Sperry JS, Christman MA, Choat B, Rabaey D, Jansen S (2011) Testing hypotheses that link wood anatomy and ultrastructure to cavitation resistance in the genus *Acer*. New Phytol 190:709–723.
Li S, Lens F, Espino S, Karimi Z, Klepsch M, Schenk HJ, Schmitt M, Schuldt B, Jansen S (2016) Intervessel pit membrane thickness as a key determinant of embolism resistance in angiosperm xylem. IAWA J 37:152–171.
Liu M, Pan R, Tyree MT (2018) Intraspecific relationship between vessel length and vessel diameter of four species with long-to-short species-average vessel lengths: further validation of the computational algorithm. Trees 32:51–60.
Morris H, Plavcová L, Cvecko P et al. (2016) A global analysis of parenchyma tissue fractions in secondary xylem of seed plants. New Phytol 209:1553–1565.
Paligi SS, Link RM, Isasa E, Bittencourt P, Cabral JS, Jansen S, Oliveira RS, Pereira L, Schuldt B (2021) Accuracy of the pneumatic method for estimating xylem vulnerability to embolism in temperate diffuse-porous tree species BioRxiv. https://doi.org/10.1101/2021.02.15.431295.
Pereira L, Bittencourt PRL, Oliveira RS, Junior MBM, Barros FV, Ribeiro RV, Mazzafera P (2016) Plant pneumatics: stem air flow is related to embolism–new perspectives on methods in plant hydraulics. New Phytol 211:357–370.
Pereira L, Bittencourt PRL, Pacheco VS et al. (2020) The pneumatron: An automated pneumatic apparatus for estimating xylem vulnerability to embolism at high temporal resolution. Plant Cell Environ 43:131–142.
Pereira L, Bittencourt PRL, Rowland L, Brum M, Miranda MT, Pacheco VS, Oliveira RS, Machado EC, Jansen S, Ribeiro RV (2021) Using the pneumatic method to estimate embolism resistance in species with long vessels: a commentary on the article "A comparison of five methods to assess embolism resistance in trees". For Ecol Manage 479:118547. https://doi.org/10.1016/j.foreco.2020.118547.
Scholz A, Rabaey D, Stein A, Cochard H, Smets E, Jansen S (2013) The evolution and function of vessel and pit characters with respect to cavitation resistance across 10 *Prunus* species. Tree Physiol 33:684–694.
Sergent AS, Varela SA, Barigah TS et al. (2020) A comparison of five methods to assess embolism resistance in trees. For Ecol Manage 468:118175. https://doi.org/10.1016/j.foreco.2020.118175.
Sorz J, Hietz P (2006) Gas diffusion through wood: implications for oxygen supply. Trees 20:34–41.
Sperry JS, Hacke UG, Wheeler JK (2005) Comparative analysis of end wall resistivity in xylem conduits. Plant Cell Environ 28:456–465.
Sperry JS, Hacke UG, Pittermann J (2006) Size and function in conifer tracheids and angiosperm vessels. Am J Bot 93:1490–1500.
Torres-Ruiz JM, Cochard H, Choat B et al. (2017) Xylem resistance to embolism: presenting a simple diagnostic test for the open-vessel artefact. New Phytol 215:489–499.
Trabi CL, Pereira L, Guan X, Miranda MT, Bittencourt PRL, Oliveira RS, Ribeiro RV, Jansen S (2021) A user manual to measure gas diffusion kinetics in plants: pneumatron construction, operation and data analysis. Front. Plant Sci 12:633595. https://doi.org/10.3389/fpls.2021.633595.
Tyree MT (1997) The Cohesion-Tension theory of sap ascent: current controversies. J Exp Bot 48:1753–1765.
Tyree MT, Yang S (1992) Hydraulic conductivity recovery versus water pressure in xylem of *Acer saccharum*. Plant Physiol 100: 669–676.
Tyree MT, Zimmermann MH. (2002). Xylem structure and the ascent of sap. 2nd edn. Springer, Berlin Heidelberg. https://doi.org/10.1007/978-3-662-04931-0.
Wang Y, Liu J, Tyree MT (2015) Stem hydraulic conductivity depends on the pressure at which it is measured and how this dependence can be used to assess the tempo of bubble pressurization in recently cavitated vessels. Plant Physiol 169:2597–2607.
Wason J, Bouda M, Lee EF, McElrone AJ, Phillips RJ, Shackel KA, Matthews MA, Brodersen C (2021) Xylem network connectivity and embolism spread in grapevine (*Vitis vinifera* L.). Plant Physiol 186:373–387.
Wei C, Tyree MT, Steudle E (1999) Direct measurement of xylem pressure in leaves of intact maize plants. A test of the cohesion-tension theory taking hydraulic architecture into consideration. Plant Physiol 121:1191–1205.
Wheeler JK, Sperry JS, Hacke UG, Hoang N (2005) Inter-vessel pitting and cavitation in woody Rosaceae and other vesselled plants: a basis for a safety versus efficiency trade-off in xylem transport. Plant Cell Environ 28:800–812.
Wheeler JK, Huggett BA, Tofte AN, Rockwell FE, Holbrook NM (2013) Cutting xylem under tension or supersaturated with gas can generate PLC and the appearance of rapid recovery from embolism. Plant Cell Environ 36:1938–1949.
Yang S, Tyree MT (1992) A theoretical model of hydraulic conductivity recovery from embolism with comparison to experimental data on *Acer saccharum*. Plant Cell Environ 15:633–643.
Zanne AE, Westoby M, Falster DS, Ackerly DD, Loarie SR, Arnold SEJ, Coomes DA (2010) Angiosperm wood structure: Global patterns in vessel anatomy and their relation to wood density and potential conductivity. Am J Bot 97:207–215.
Zhang Y, Lamarque LJ, Torres-Ruiz JM et al. (2018) Testing the plant pneumatic method to estimate xylem embolism resistance in stems of temperate trees. Tree Physiol 38:1016–1025.
Zhang Y, Carmesin C, Kaack L et al. (2020) High porosity with tiny pore constrictions and unbending pathways characterise the 3D structure of intervessel pit membranes in angiosperm xylem. Plant Cell Environ 43:116–130.
Zimmermann MH, Tomlinson PB (1966) An analysis of complex vascular systems in plants: optical shuttle method. Science 152: 72–73.

Downloaded from https://academic.oup.com/treephys/article/43/1/88/6682843 by BIBLIOTECA CENTRAL UNIV ESTADUAL CAMPINAS user on 06 February 2025